Understand and characterize draining of acid milk gels using Magnetic Resonance Imaging and Time Domain-Nuclear Magnetic Resonance

Tatiana Monaretto, Stephane Quellec, Mireille Cambert, Romain Richoux, Janushan Christy, Patrice Gaborit, Marie-Helene Famelart, Corinne Rondeau-Mouro

Journal of Food Engineering 377 (2024) 112088

Contents lists available at ScienceDirect

Journal of Food Engineering

journal homepage: www.elsevier.com/locate/jfoodeng

Understand and characterize draining of acid milk gels using Magnetic Resonance Imaging and Time Domain-Nuclear Magnetic Resonance

Tatiana Monaretto [a], Stéphane Quellec [a], Mireille Cambert [a], Romain Richoux [b], Janushan Christy [c], Patrice Gaborit [d], Marie-Helene Famelart [e], Corinne Rondeau-Mouro [a,*]

[a] INRAE, UR OPAALE, 17 Avenue de Cucillé, CS 64427, 35044, Rennes Cedex, France
[b] ACTALIA, Produits Laitiers, 65 rue de Saint Brieuc, BP 50, 35009, Rennes Cedex, France
[c] ACTALIA, Expertise Analytique Laitière / Cecalait, 419 route des champs laitiers, CS 50030, 74801, La Roche sur Foron, France
[d] ACTALIA, Site ENILIA-ENSMIC, 1 rue des Babigeots, 17700, Surgères, France
[e] INRAE-L'Institut Agro Rennes-Angers, UMR STLO, Rennes, France

ARTICLE INFO

Keywords:
Acid-gel draining
Serum
Self-diffusion
Relaxation time
Kinetics of draining
Imaging

ABSTRACT

A novel dedicated device is introduced to enable investigation of the filtration draining process of different acid-induced milk gels using Magnetic Resonance Imaging (MRI). This approach allows the spatio-temporal resolution of serum content and distribution in gels throughout draining. Its application for the characterization of five acid gels formulated using reconstituted or fresh milk and using different thermal treatments and/or lactic starters indicates its large potential for a better understanding of acid-induced gel draining in dairy industry. Self-diffusion and relaxation measurements using Time Domain-Nuclear Magnetic Resonance (TD-NMR) were performed on the gels following filtration draining to validate and supplement the MRI results, while gels obtained through centrifugation were examined in view of correlating T_2 relaxation times to the water content of gels. The presence of lipids in reconstituted milk or the substitution of a casein fraction by microparticulated denatured whey proteins were shown to impact the structure of gels and their serum holding capacity.

1. Introduction

Acid-induced milk gels are widely produced and consumed worldwide. Their popularity can be attributed, in part, to the various health claims and potential therapeutic benefits associated with their consumption (Lucey and Singh, 1997; Wang and Zhao, 2022). It is no easy task, though, to ensure the quality and stability of these gels, since multiple variables are involved in their production, not least the draining process, which is vital to the creation of high-quality and stable gel-based dairy products. An understanding of the factors that affect drainage in milk acid gels (the presence of soluble and/or aggregated serum proteins, the lipid concentration, the bacterial strain used (mesophilic or thermophilic) and the draining pH) can thus be useful in improving product quality, developing new formulations, optimizing manufacturing processes, maintaining consistency, and extending shelf life (Lucey, 2002, 2017; Lucey and Singh, 1997). Yet the methods currently used to study the draining process are relatively limited in their scope. They generally adopt approaches that do not provide detailed insights into the gel's behavior during mechanical draining (Daviau et al., 2000). Moreover, in industrial production, the management of acid gel draining often relies on experience and practical knowledge rather than a systematic technological approach. Corrective actions are typically taken after drainage delays have occurred.

Final microstructure provides a valuable indicator of quality in fermented milk products, directly affecting their texture, appearance, and sensory properties. Scanning electron microscopy (SEM) and confocal laser scanning microscopy (CLSM) are commonly used in the dairy industry to observe acid gel microstructure (Wang and Zhao, 2022). However, most of these techniques provide surface information or a restricted field of view, with only a limited capacity to study the internal structure or depth-related features of samples. Consequently, despite the increasing number of studies on milk acid gel production, there is still a lack of the specialized techniques required to comprehensively address and efficiently control its production process, particularly those that can offer real-time and non-destructive observations.

Time Domain-Nuclear Magnetic Resonance (TD-NMR) and Magnetic Resonance Imaging (MRI) have both shown promise as non-invasive tools to characterize dairy products, understand dairy engineering,

* Corresponding author.
E-mail address: corinne.rondeau-mouro@inrae.fr (C. Rondeau-Mouro).

https://doi.org/10.1016/j.jfoodeng.2024.112088
Received 6 October 2023; Received in revised form 4 April 2024; Accepted 7 April 2024
Available online 8 April 2024

and provide valuable information about the composition and internal structure of the product. Applying these techniques to dairy products involves the investigation of the sensitivity of relaxation times to chemical composition, water content, and changes in protein structure and pH (Le Dean, Mariette and Marin, 2004; Mariette, 2006a, 2006b; Mariette et al., 1993; Métais et al., 2006).

Numerous studies have reported the use of relaxation measurements by TD-NMR to interpret the microscopic structure of the water compartment inside the dairy matrix (Chen et al., 2020; Pocan and Oztop, 2022; Tellier et al., 1993). Transverse relaxation times (T_2) from serum water have also proved valuable in monitoring age-related changes in Mozzarella samples (Gianferri, D'Aiuto, Curini, Delfini and Brosio, 2007). In addition to the investigation of relaxation times, water diffusion experiments offer a unique method of investigating changes in water mobility. The information they provide concerns network tortuosity, adding significant detail to our knowledge of gel network structure (Bouchoux et al., 2012; Colsenet et al., 2005; Salami et al., 2013; Smith et al., 2017; Vogt et al., 2015).

MRI, too, has proven to be a valuable technique for the study of dairy products, for example, establishing the effects of freezing on mozzarella cheeses through the mapping of T_2 distributions (Kuo et al., 2003), and analyzing the ripening stage of Grana Padano cheese (Mulas et al., 2016). Despite the wide range of possible MRI applications, this potential has nevertheless been little explored in the study of dairy products. This is certainly true of the investigation of the draining process by MRI, where only a few studies have been conducted. In these studies, MRI was employed to determine water distribution during the draining of the curd (Mariette, 2006a).

The present study was designed to investigate the draining process in differently formulated acid gels using MRI and NMR techniques. These formulations have been chosen amongst 45 others, because of their contrasted behaviors in draining. Two draining methods have been studied. In the first, gravimetric forces were applied through a filter thanks to a partial vacuum (we call this method filtration draining), while in the second, centrifugation was applied for selected durations. A unique experimental approach was applied for the first time in this investigation and a novel dedicated device was created to conduct MRI measurements. These enabled us to assess both gel water distribution and the serum content drained during filtration with a vacuum system. To validate and complement the MRI results, additional diffusion and relaxation measurements using TD-NMR were performed on the final gels (i.e., at the end of filtration draining). Last, we studied the drained gels obtained through centrifugation using TD-NMR measurements. The results obtained from filtration draining and centrifugation were compared and discussed.

2. Material and methods

2.1. Gel formulations and preparation

Table 1 shows the composition, thermal processing conditions and microorganisms used to prepare acid gels. Gels 24, 29, and 34 were formulated using reconstituted milk, while gels B and D were prepared using fresh milk. The values of the native soluble whey protein contents of gels B and D are close to those shown in Table 1, representing the typical composition of fresh skimmed milk. In gels 29 and D, microparticulated denatured whey protein was added as a substitution for the casein fraction. For further information on gel formulation and preparation, please refer to Section S1 of Supplementary Material.

After incubation, the coagulum was stirred in a curd-stirrer for 5 min at 350 rpm and then recirculated using a peristaltic pump. The coagulum obtained at the end of this process is referred to in the present study as non-drained (ND) gel. The ND gels were then transferred into either centrifuge tubes to be drained by centrifugation or into the MRI prototype system for filtration-based draining at 20 °C. Centrifugation draining was performed at the acidification temperature of 2800 *g* for 3, 7, 15, and 30 min. The supernatant or serum was removed, while the pellet or gel was used in the investigation of draining.

The water and dry matter contents were determined for each gel. See Supplementary Material, section S2 and Fig. S2 for description and discussion of the results.

2.2. MRI experiment: filtration draining

2.2.1. Device to monitor the filtration draining process

The experiments were conducted on a whole-body Siemens MRI operating at 1.5 T and using a head coil, as illustrated in Fig. 1. A filtration system was developed to monitor the real-time filtration draining process and conduct the experiments under repeatable, controlled, and automated conditions. This device produced in the laboratory were constructed with plastic and Teflon amagnetic materials compatible with MRI equipment, and their size and shape were adapted to the head coil. A lab-built holder made up of Teflon was specifically designed to accommodate four filtration flasks within the head coil. In the present work, the filtration device consisted of two plastic flasks (diameter 52 mm and height 70 mm), each containing an upper chamber where the gel was placed and a lower chamber in which the serum was collected during filtration (depicted in Fig. 2 (a)). The two parts of the flasks were connected by a Teflon threaded junction housing a filter. Filtration draining was carried out using a vacuum system at 20 °C. The vacuum pressure setting is confidential industrial information.

Table 1
Parameters and milk formulations used to prepare gels for NMR-MRI analysis. Gels 24, 29, and 34 were made with reconstituted milk, while gels B and D were made with fresh skimmed milk.

Variant	PC (g/Kg)	NSSP_PC (%)	DWPP_PC (%)	LC_PC	HTT (°C)	D_TT (sec)	LST	ACT (°C)	pHDR
24	44	30	0	0	72	120	Mesophilic	25	4.6
29	32	15	12.5	0	95	20	Mesophilic	35	4.6
34	44	15	0	0.8	95	120	Thermophilic	35	4.2
B	~32[a]	~20[a]	0	0	95	120	Mesophilic	25	4.6
D	~32[a]	~20[a]	12.5	0	95	120	Mesophilic	25	4.6

PC – Protein content.
NSSP_PC - Percentage of native soluble serum protein to protein content.
DWPP_PC – Percentage of denatured whey protein particles (mean size 2–200 μm, macroparticles) to protein content.
LC_PC – Ratio of lipid content to protein content.
HTT – Heat treatment temperature.
D_TT – Duration of thermal process.
LST – Lactic starter type.
ACT - Acidification temperature.
pHDR – pH of draining.
[a] Approximate quantity in fresh milk – No added proteins, lipids, or native soluble serum protein.

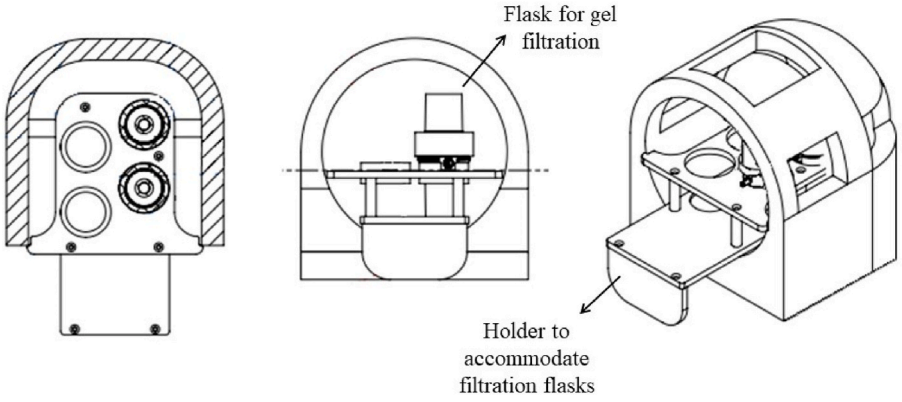

Fig. 1. Device used to monitor the filtration draining process using MRI: (a) top view, (b) profile view, (c) overview.

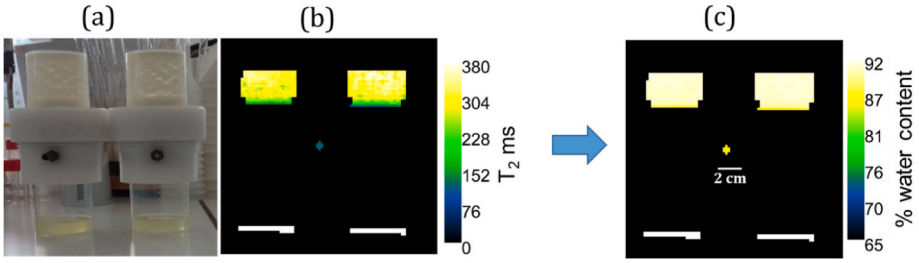

Fig. 2. (a) Photo of the device developed to monitor the filtration draining process using MRI. This image shows the two flasks at the end of the draining experiment, with the upper chamber containing the drained gels and the lower chamber holding the drained serum. A threaded section connects the two parts. (b) T_2 map and (c) water content map. The small shape at the center of each map is produced by the dopped water control tube.

2.2.2. MRI protocol and data processing

A multi-contrast spin-echo sequence was used to acquire 128 images (128 echoes) with an echo time of 5 ms, enabling the calculation of T_2-weighted images. Images were acquired using a sagittal section, with a slice thickness of 5 mm, a voxel size of 2 mm × 2 mm × 5 mm, and a field of view (FOV) of 192 mm^2. The repetition time (TR) was set to 1.5 s, and the duration was approximately 2 min and 24 s. These parameters were chosen to optimize experimental time and run several acquisitions during draining, particularly in the initial stages where the changes were more significant. A total of 23 acquisitions were run during the filtration draining process. The first 16 acquisitionswere run consecutively without waiting, while there was a 15 min waiting time between runs from the 17th to the 23rd acquisition. The overall duration of the MRI session for each draining process was around 2h20min.

A macro was developed by the team using Scilab to fit the T_2 data. Each voxel was fitted via this macro using a single exponential decay model (equation (1)):

$$I(t) = I_{(0)} e^{\left(-TE/T_2\right)} \quad (1)$$

Here, I(t) is the observed transverse magnetization at a given time (t), $I_{(0)}$ is the equilibrium magnetization (proportional to the liquid proton density), TE is the echo time, and T_2 is the transverse relaxation time. The fitting of the 128 echo images enabled the spatially distributed T_2 and I_0 values to be mapped. The T_2 images were generated using the ImageJ program.

Calculation of the water-weighted images has been performed based on the method described by Mariette et al. (Mariette et al., 1999).

The height of the white image in the lower chamber of each flask (Fig. 4 at 2h20) could be directly correlated with the weight of the serum collected at the end of the draining experiment. The percentage of serum drained during each image acquisition was calculated by dividing the total amount of drained serum by the amount of initial gel.

2.2.3. Fitting of kinetics by a logarithmic model

The data of the drained serum evolution (in percentage) against time were fitted by a logarithmic model (equation (2)):

$$P_t = \begin{cases} 0 & P_t \leq 0 \\ a_0 + a_1 \times \log(t) + e_t & 0 < P_t < 1 \\ 1 & P_t \geq 1 \end{cases} \quad (2)$$

where P_t is the percentage of the drained serum, a_0 and a_1 are the parameters of the logarithmic model and t is the time in hours.

The estimations of the logarithmic model parameters were carried out using the SAS software "nlmixed" procedure (SAS Institute Inc, 2015). These parameters were determined by minimizing the loss of information between various models. AIC, the Akaike information criterion (Akaike, 1998) was used to carry out this comparison. The best model is that with the lowest AIC value.

2.3. NMR experiment

All NMR analysis was conducted on minispec spectrometer (Bruker, Wissembourg, France) operating at 0.47 T (20 MHz). The measurements were performed at 20 °C on non-drained, centrifuged and gels obtained by filtration. This gel, that was monitored by MRI is described as 'filtration gel'. Analysis was carried out using NMR tubes with an approximate diameter of 10 mm. The tubes were filled with approximately 1 cm of gel.

2.3.1. Transverse relaxation

Free induction decay (FID) and Carr–Purcell Meiboom–Gill (CPMG) were used to measure the transverse relaxation time. The FID signal was acquired from 11 to 151 μs, one point every 0.4 μs. The CPMG signal was obtained using a pulse sequence spacing of 100 μs between 90 and 180° (τ); the number of scans was 8, the recycle delay and the number of echoes were adjusted as required for each sample, with a range of 2–8 s

(set at $5T_1$) and 1500–10,000 echos, respectively.

The T_2 distribution spectrum was used to help establish an a priori estimate of the number of relaxation components in the data. The T_2 spectrum was obtained using the inverse Laplace transform based on the maximum entropy method (Mariette et al., 1996). The FID-CPMG signals were then fitted applying the Levenberg-Marquardt method to four relaxation time components, as described by equation (3):

$$I(t) = I_{(1)}e^{\left(-t/T_{21}\right)^2} + I_{(2)}e^{\left(-t/T_{22}\right)^2} + I_{(3)}\,e^{-t/T_{23}} + I_{(4)}e^{-t/T_{24}} + c(t) \quad (3)$$

where I(t) is NMR signal intensity at a given t, $I_{(i)}$ and T_{2i} are the intensity and spin-spin relaxation time of each relaxation component, respectively, and c(t) is the residual error.

Relative intensities (I - %) were calculated for each component (I(1), I(2), I(3), and I(4)). The weighted average $T_2(3 + 4)$ was determined using the T_2 values and intensities (I) of components 3 and 4. It was calculated using the following formula:

$$T_2(3+4) = ((T_{23} * I(3)) + (T_{24} * I(4))) / (I(3) + I(4)) \quad (4)$$

Error bars in the relaxation graphics designate the experimental repeatability of the two samples.

2.3.2. Diffusion

A pulsed-field-gradient stimulated-echo (PFG-STE) sequence, as described by Tanner (1970), was used to measure the water self-diffusion coefficient in gels (Tanner, 1970). Pulse field strength gradients were calibrated using a sample of pure water with a known self-diffusion coefficient (1.99×10^{-9} m^2 s^{-1}) at 20 °C. The self-diffusion coefficients were determined using equation (5) where E is the echo intensity during gradient pulses ($I(2n\tau)_g$) divided by the echo intensity with no gradient ($I_0(2n\tau)_{g=0}$):

$$E = \frac{I(2n\tau)_g}{I_0(2n\tau)_{g=0}} = \exp(-\gamma^2 g^2 \delta^2 (\Delta - \delta/3) D) \quad (5)$$

In equation (5) g is the gradient pulse strength, δ and Δ are the gradient pulse length and distance between the leading edges of the pulse gradients respectively, γ is the gyromagnetic ratio (for protons, γ - 26.7520×10^7 $radT^{-1}$ s^{-1}), and D is the water self-diffusion coefficient.

The PFG-STE sequence was repeated for ten different g values for each experiment while δ and Δ remained fixed. The ten gradient strengths, g, were: 0.4, 0.80, 1.20, 1.40, 1.95, 2.10, 2.30, 2.70, and 2.89 T/m. Sixteen scans were carried out, and the recycle delay was set at $5T_1$ (as for the transverse relaxation measurements). Δ and δ were measured over 5–200 ms and 0.545–0.085 ms, respectively.

The error bars shown in the diffusion coefficients of gels 34, B, and D indicate the experimental repeatability of the two samples. Diffusion measurements for gels 24 and 29 were not repeated due to restricted experimental time during the week of analysis; their diffusion coefficients therefore have no error bars.

3. Results and discussion

3.1. MRI experiments

3.1.1. Calculation of T_2 and water content maps

Fig. 2b provides an example of a T_2-weighted image obtained during filtration. The color contrast in the image corresponds to different T_2 values, as indicated in the color bar. A color scale that ranges from dark blue (representing short T_2 values < 75 ms) to light yellow (indicating long T_2 values > 300 ms) has been selected to demonstrate the variability of T_2 within the gel.

Relaxation time varies according to the position within the sample, which is influenced by sample composition, particularly water content. In Fig. 2b, the yellow pixels in the images of the upper chambers of the two flasks show gel distribution, while the green pixels represent the gel located close to the filter in the threaded portion (Teflon section in Fig. 2a), which has lower T_2 values. The white pixels at the bottom of the image correspond to the drained serum and exceed the limit of the chosen scale for T_2 on the color bar, with a T_2 value of approximately 900 ms.

The use of the relaxation time T_2 as a water content indicator presupposes the realization of a calibration model on the whole range of water content variation. This was realized using MRI T_2-weighted maps and T_2 relaxation times measured by TD-NMR on non-drained and centrifuged gels (3 min, 7 min, 15 min, and 30 min) (Mariette, 2004, 2006a). This calibration procedure allowed the calculation of water content maps of drained gels by filtration as illustrated in Fig. 2b and c.

3.1.2. Interpretation of the MRI data

Fig. 3 shows space-time-resolved images of water content during the filtration draining process of all studied gels. These images allow the progression of the draining process to be observed, with colors representing different water content levels. Water content decreases from light yellow to dark blue, as shown in the calibration bar in the bottom-right corner of Fig. 3. The serum image (white area at the bottom of each image in Fig. 3) was used to determine the percentage of serum drained throughout the experiment, as illustrated in Fig. 4.

Fig. 4 shows that gel 34 had the lowest water content during the initial stages of the draining process. At 5 min, a significant portion of gel 34 appears in dark yellow, indicating approximately 88% water content, whereas the other gels are mainly in light yellow-white shades, indicating around 90% water content. This observation is in line with the information for ND gels in the Supplementary material (Fig. S2), where ND gel 34 exhibits the lowest water content (88 ± 0.01%). Moreover, the draining process for gel 34 was the slowest compared to the other gels. Water content decreased more slowly in the upper chamber of the flask for gel 34 than in the others, as depicted in Fig. 3. At 20 min, we also observed a more prominent water gradient in gel 34. The network appeared much denser near the filter, leading to limited draining and causing clogging. At 20 min, the gradient of gel 34, located close to the filter, ranges from green to dark blue, indicating a water content of approximately 81%–70%. By contrast, the pixels of other gels in this area are mostly green, suggesting a water content of around 81%. This fits with the quantity of serum drained during the experiment, which is lower for gel 34 (56 %) than for other gels (79–85 %), as shown in Fig. 4. It is worth noting that gel 34 contains lipids, which suggests that the conversion of T_2 to water content in Fig. 3 may not be entirely accurate. Nevertheless, despite the potential inaccuracy of this water content measurement, we can still assume that lipids have an impact on the draining process, resulting in a slower draining rate. These findings are in line with the literature, highlighting the substantial contribution of fat to the rennet gel's structure and, consequently, its water-holding capacity (Métais et al., 2006).

In contrast to gel 34, the kinetic draining process for gels 24 and 29 was the most rapid, with the serum draining faster than in other gels (Fig. 4). Between 10 and 65 min of draining, the quantity of serum drained from gel 24 was slightly higher than for gel 29. However, after 75 min, the serum drained content was similar in both gels, as shown in Fig. 4. Likewise, at the end of this draining experiment, gels 24 and 29 exhibited similar levels of drained serum (about 76 g - Fig. 4) and gel water content (around 70 and 72%, Fig. 3 and Supplementary Material Fig. S2).

Despite the similarity in gel composition, the serum drained faster from gel D than B (Fig. 4). Additionally, in Fig. 3, at 50 min, gel D can be seen to have a slight lower water content (ranging from yellow to light green pixels - 88%–80%) than gel B (ranging from light yellow to light green pixels - 90%–80%). However, at the end of the experiment, both gels reached similar levels of water content (around 75 and 77 % Fig. 3 and Supplementary Material Fig. S2) and drained serum content (around 79 % - Fig. 4). It suggests that the presence of microparticulated

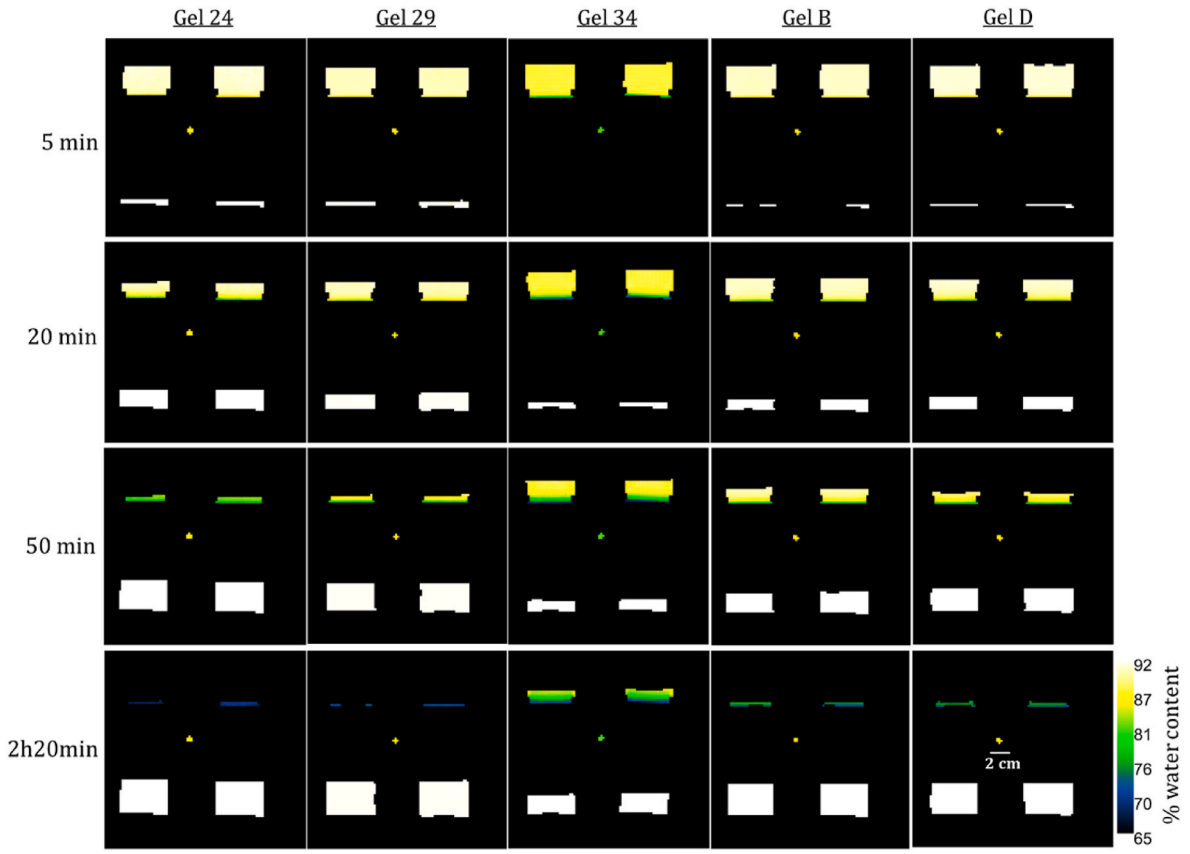

Fig. 3. Water content maps for gels 24, 29, 34, B, and D at different draining times: around 5 min, 20 min, 50 min, and 2h20min. The small shape in the center is produced by the dopped water control tube.

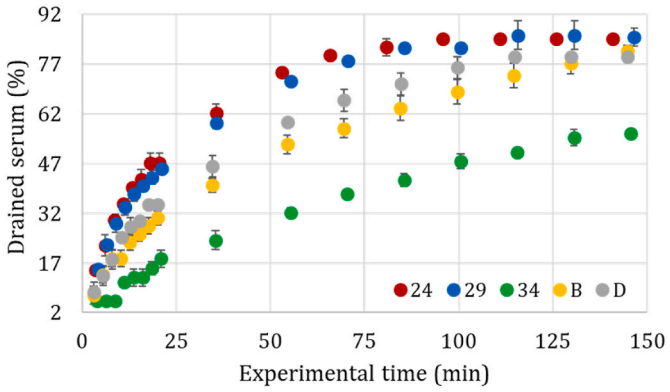

Fig. 4. Drained serum (%) over the experimental time (min) for gels 24, 29, 34, B, and D.

denatured whey protein in gel D influenced its draining kinetics, resulting in a faster rate compared with gel B. Despite this, the MRI images show that the structure of both gels is similar at the end of the filtration draining experiment.

It is worth noting that at the end of filtration draining, gels B and D (79 %) had produced slightly less drained serum than gels 24 and 29 (85 %) (Fig. 4); consequently gels B and D exhibited slightly higher water content (around 75 and 77 %, Fig. 3 and Fig. S2 in Supplementary material) than gels 24 and 29 (around 70 and 72% - Fig. 3 and Fig. S2 in Supplementary material). Meanwhile, the draining process displayed significantly faster kinetics for gels 24 and 29 than for gels B and D (Fig. 4). This difference in draining kinetics may be attributable to different thermal treatments. Gels 29 and 24 underwent milder thermal treatments (95°C/20 s and 72°C/120 s, respectively) compared to gels B and D (95°C/120 s) (Table 1), which may have reduced the water-holding capacity of gels 29 and 24. It is important to note that as the intensity of the thermal treatment increases, an increase can also be observed in the denaturation of the protein structure, potentially leading to higher water-holding capacity (Vasbinder et al., 2003).

In order to get comparable numerical data, each kinetics reported in Fig. 4 was fitted by a logarithmic model (Fig. S1 and Table S1 in Supplementary material). As the estimated a_1 parameters were quite similar whatever the gel, the kinetics were fitted by estimating a single value of 0.199 for a_1. In this condition, the differences between each curve were the starting point of the draining and the parameter a0 which varied from 0.406 to 0.713. Table 2 reports the estimated time (in hour) necessary to get a percentage of 5, 50 or 95 % of drained serum. The draining level associated with gels 24 and 29 are the fastest. With these gel formulations, 5% of the serum is drained after 0.04 h. It takes around 0.34 h to 0.38 h to drain 50% of the total serum and 3.29 h to 3.65 h to get 95% of the total serum. The draining level associated with gel 34 is the slowest. After 0.17 h, 5% of the serum is drained while 95% of serum could be obtained after 15 h.

Table 2
Results of the estimation (in ascending order) of the time required to reach a draining percentage of 5, 50 or 95% of the total drained serum in gels 24, 29, 34, B and D.

Gel	5%	50%	95%
24	0.04	0.34	3.29
29	0.04	0.38	3.65
D	0.06	0.57	5.46
B	0.07	0.70	6.70
34	0.17	1.60	15.34

The following section provides a thorough discussion of the structures of the filtrated and centrifuged gels, based on interpretation of the T2 and diffusion coefficients measured by TD-NMR.

3.2. TD-NMR measurements

3.2.1. Changes in transverse relaxation times

An illustration of the evolution of T_2 relaxation times during the different draining processes is provided in Fig. 5 for gel D. The most intense and longest T_2 in Fig. 5b decreases with increased centrifugation time. It ranges from 391.7 ms for the ND sample to 91.2 ms and 44.0 ms respectively for 3 min and 30 min of centrifugation. Additionally, the contribution of the relative area to this normalized signal, correlated with proton density, decreases from 0.98 for the ND sample to 0.88 for the 30 min sample. For the filtered gel D, this longest T_2 component has a value of 51.7 ms and a relative area of 0.9, comparable to the centrifuged sample at 15 min.

The T_2 component with the highest value in dairy products is mainly attributed in the literature to exchangeable protons from two different chemical environments within the aqueous phase of the casein dispersion. One of these environments is commonly associated with the water in the "junction zone," where water molecules interact strongly with protein chains. The other proton environment is created by the interconnected mesh-like network formed by casein, and is often referred to as "entrapped water." Under fast diffusion exchange conditions, these two components should merge into a single component (Gianferri et al., 2007; Hansen et al., 2010; Hinrichs et al., 2004; Le Dean et al., 2004; Mariette et al., 1993).

Fig. 5 presents the evolution of the T_2 relaxation times measured for the non-drained and drained gel D. For the ND gel, two components (under slower diffusion exchange conditions) can be seen in Fig. 5b, which then merge into a more extended component for centrifuged and filtered samples (faster diffusion exchange). However, when the Levenberg-Marquart method is used in processing the data, two components are identifiable consistent with a regime of slow diffusive exchange between two water phases (T_{23} and T_{24}). This result is coherent with data in the literature showing that some water molecules are to be found in junction domains, while others can be trapped inside the gel mesh (Anedda et al., 2021; Hills et al., 1990; Mariette, 2006b, 2017).

For ND and drained gels, a T_2 component was identified between 0.5 and 5 ms (asterisk in Fig. 5a) but, because of its low intensity, it was not investigated. The contribution to the total NMR signal of the two shortest T_2 components ($T_{21} \sim 0.02$ and $T_{22} \sim 0.1$ ms) in Fig. 5a increased with centrifugation time. Possible candidates for these two relaxation components can be found in the literature. Bouchoux et al. (2012) has reported a single T_2 component associated with non-exchangeable protein protons in the casein dispersion at 25 °C. The native phosphocaseinate dispersion showed a T_2 range of 0.02–0.03 ms at concentrations of 20–150 g/L, while in the sodium caseinate, T_2 had a range of 0.1–0.2 ms at concentrations of 80–100 g/L. These findings were attributed to the differences in structure and organization between the two types of casein dispersion and to the influence of concentration on organization (Bouchoux et al., 2012). In antother hand, Gianferri et al. (2007) has described two T_2 components at 7.3 ms (junction zone water) and 47 ms (entrapped water) for fresh Mozzarella (Gianferri et al., 2007).

The relative intensities of the T_{21} and T_{22} components were correlated with dry matter, while those from T_{23} and T_{24} were correlated with water content, as shown in Table S2 (Supplementary material, section S3). I(1 + 2) and I(3 + 4) were found to correlate well with dry matter and water content, respectively. On this basis, the following subsections, 3.2.1.1 and 3.2.1.2, discuss the components in relation to dry matter and water content.

3.2.1.1. Evolution of T_{21} and T_{22} components. Fig. 6 shows the weighted average of T_{21} and T_{22} (a) and I(1 + 2) (b) for three gel states: ND, drained by centrifugation, and drained by filtration. T_{21} remains relatively unchanged across all gels, while T_{22} slightly decreases or increases with the draining process (Fig. 6a). Assuming that these two components

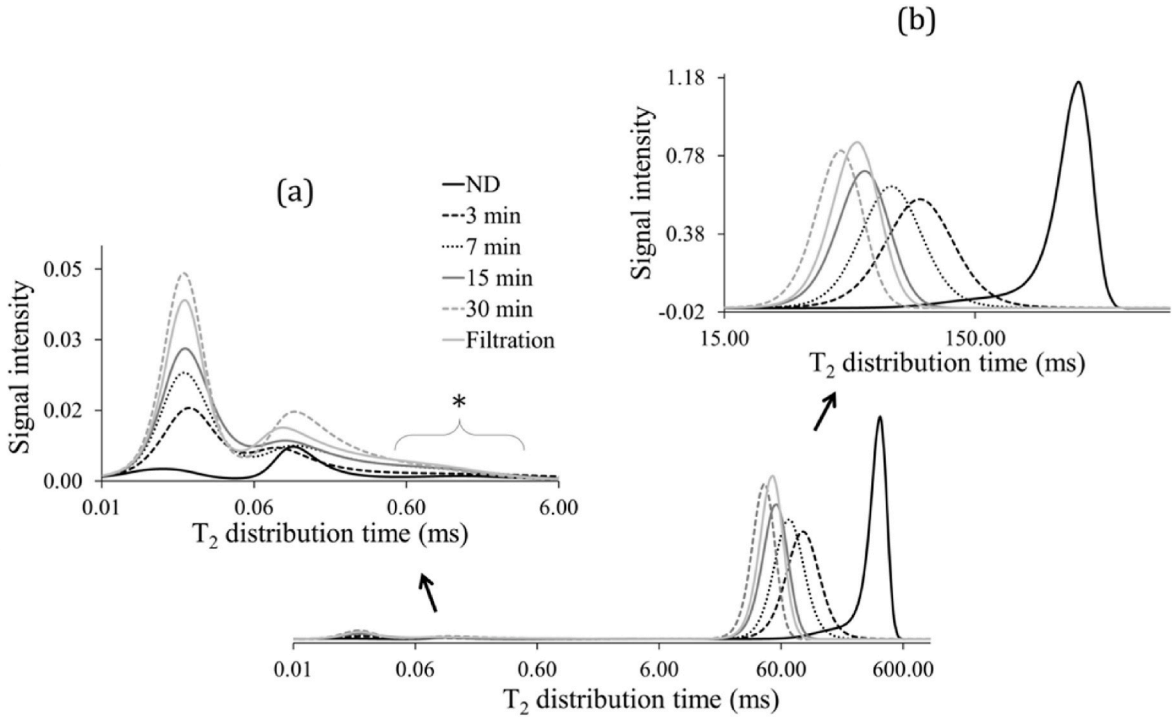

Fig. 5. T_2 distribution of gel D for the non-drained sample (black line) and samples drained by centrifugation (3 min – black dashed line, 7 min – black dotted line, 15 min – gray line, and 30 min – gray dashed line) and filtration (light gray line). Zooms of the shortest and longest T_2 components are shown on the top left (a) and top right (b) respectively. * indicates a T_2 component of 0.5–5 ms.

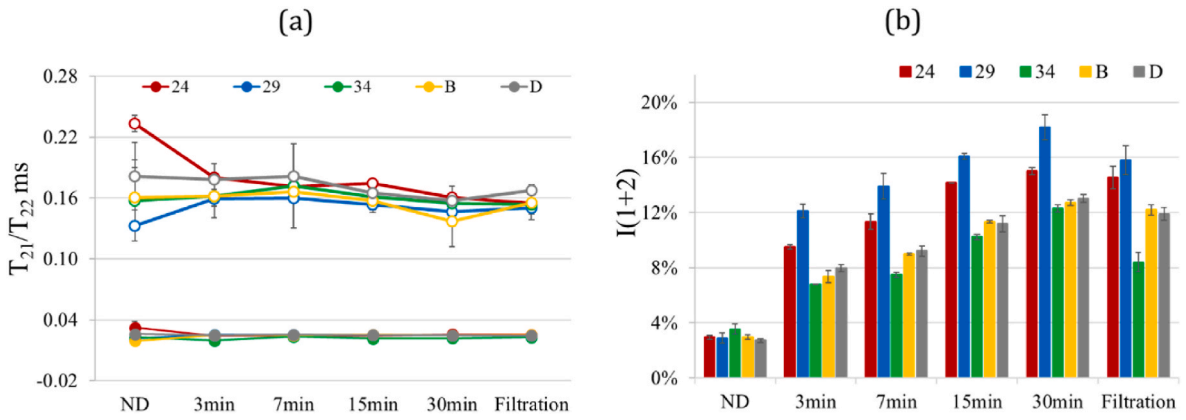

Fig. 6. T_{21} (solid symbols) and T_{22} (outline symbols) are shown in (a), and I(1 + 2) is shown in (b) for ND, centrifuged, and filtered samples of gels 24 (red), 29 (blue), 34 (green), B (yellow), and D (gray).

derive from protein protons, as explained above (Bouchoux et al., 2012; Le Dean et al., 2004; Mariette et al., 1993), the decrease in the related relaxation times can be attributed to the impact of protein aggregation on dipole-dipole interactions between protein protons, which are no longer efficiently averaged due to their limited rotational motion (Colsenet et al., 2005). Interestingly, in gel 24, T_{22} appears to decrease slightly after centrifugation and filtration, suggesting an increase in protein assemblies due to serum release. However, in view of the standard error of T_{22}, this hypothesis is difficult to maintain for all the gels.

The contribution of I(1 + 2) increased with centrifugation time for all gels, in agreement with the incremental increase in dry matter content (Fig. 6b). Centrifuged and filtered gels 24 and 29 had the highest I(1 + 2) values (Fig. 6b), indicating a higher dry matter content than the other gels. This may be attributable to differences in thermal treatment temperature and duration. In the case of gel 24, a temperature of 72 °C was maintained for 120 s, while gel 29 was held at 95 °C for 20 s. By contrast, all other gels were treated at 95 °C for 120 s (Table 1). As a result, gel 29 and gel 24 underwent less severe thermal treatment, leading to lower denatured protein levels and water holding capacity. The lower water content of these gels produced a proportionately higher dry matter content. Meanwhile, gel 34, in both its centrifuged and filtrated forms, displayed the lowest I(1 + 2) values (Fig. 6b), suggesting that some of the lipids present in this gel contribute to liquid components (I(3 + 4)).

The impact of the filtration process is shown to be very similar to that of centrifugation. I(1 + 2) values in filtered gels 24, B, and D are similar to those in the centrifuged gels at 30 min, while for gels 29 and 34, they are close to those of the centrifuged gels at 15 and 7 min, respectively.

T_{21}, T_{22}, and I(1 + 2) are similar for drained and ND gels B and D (taking error bars into account – Fig. 6). This suggests that the microparticulated denatured whey proteins added as a partial substitute for casein in gel D should not impact protein proton mobility or dry matter content. These denatured whey proteins constitute the only difference between the formulations for gels B and D.

3.2.1.2. Evolution of T_{23} and T_{24} components. The separate examination of T_{23} and T_{24} (not shown here) makes no significant contribution to our understanding of gel structure. These two components are therefore discussed together, using their T_2 weighted average, $T_2(3 + 4)$.

Fig. 7a depicts the weighted average of $T_2(3 + 4)$, while I(3 + 4) is shown in Fig. 7b. The draining process decreases the relative number of protons and their mobility in pools 3 and 4, as evidenced by the reductions in I(3 + 4) and $T_2(3 + 4)$ as draining progresses. This observation suggests that the protein network is compressed during the draining process, reducing internal water concentrations and mobility within the casein aggregates.

All ND samples display similar relative intensities for I(3 + 4). However, gel 34 ND has a considerably shorter $T_2(3 + 4)$ value (233.9 ± 1.3 ms), suggesting that the mobility of protons in pools 3 and 4 is more restricted in this gel. Interestingly, when drained, gel 34 has the highest I(3 + 4) and the longest $T_2(3 + 4)$ in all instances. Additionally, during filtration draining, gel 34 behaves differently from the other gels, with significantly higher values for $T_2(3 + 4)$ (80.0 ± 7 ms) and I(3 + 4) (92 ± 1%). These results suggest that in its drained state, gel 34 contains a more significant number of mobile protons in pools 3 and 4, indicating a less compact microstructure, and this is probably related to the additional lipid content, as already discussed.

At the other end of the scale, the lowest I(3 + 4) values in Fig. 7b are recorded for drained gel 29. Additionally, the mobility of protons in pools 3 and 4 is highly restricted in this gel, as evidenced by the shortest $T_2(3 + 4)$ values in Fig. 7a. These characteristics suggest that gel 29 has a

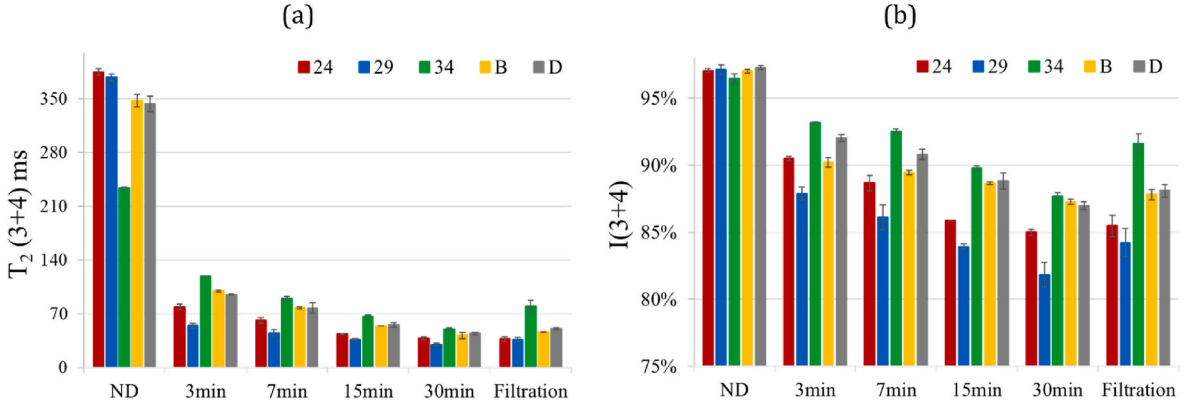

Fig. 7. (a) Weighted average of $T_2(3 + 4)$ and (b) the average of I(3 + 4) for ND, centrifuged and filtered samples for gels 24, 29, 34, B, and D.

more compact gel network that is probably related to the microparticles of denatured whey protein added to this gel, and/or to the shorter duration of its thermal treatment. Although drained gels B and D have similar $T_2(3+4)$ values, it is noteworthy that gel D displays higher I(3 + 4) values in centrifuged samples at 3 and 7 min. This suggests that denatured whey proteins (12.5%, added as a substitute for casein, see Table 1), present only in gel D, contribute to serum retention in these two particular centrifuged samples.

By studying I(3) and I(4) separately, we can better ascertain the changing relative proportions of exchangeable protons present in the junction domains and in the gel mesh for ND during draining. Relative intensities I(3) and I(4) can be seen in Figs. S3a and S3b (Supplementary material, section S4), respectively. In ND gels, I(4) is higher than I(3). This result can be explained by the fact that most of the water/serum protons are located inside the mesh of the gel network rather than in the junction zone. A clear trend can be observed for drained gels 24, 29, B, and D (see further details in Supplementary material, section S4). Interestingly, gel 34 does not follow this trend. This suggests that the protein network in gel 34 imposes no significant restrictions on water/serum mobility and that pools 3 and 4 in this gel are not associated exclusively with water-exchangeable protons but also with protons in the lipids. This hypothesis is supported by the fact that gel 34 was the only gel to which lipids were added (Table 1). Chaland et al. (2000) have also reported the presence of protons from lipids in the liquid T_2 component of cheese (Chaland et al., 2000).

3.2.2. *Evolution of the water self-diffusion coefficient*

In this last section, we investigate how water displacement is affected by a centrifugation draining time of 30 min and by differences in gel formulation. Because casein micelles are large particles with high porosity, the study of water self-diffusion in this sort of system can offer valuable structure-related insights into the impacts of gel type and draining process on diffusion. In these experiments, the distance traveled by each water molecule ($(6D\Delta)^{1/2}$) during the diffusion time (Δ) was assumed to be consistently much greater than the characteristic mean size of the reservoirs (Woessner, 1963). We recorded Δ values ranging from 5 to 200 ms, corresponding to diffusion distances of 5–35 μm ($(6D\Delta)^{1/2}$) (Callaghan et al., 1983; Colsenet et al., 2005).

The water self-diffusion coefficient for gels is commonly expressed in D_{app}, which is obtained by dividing D, the self-coefficient of water in the gel, by the self-diffusion of free water at 20 °C (D_0 - 1.99 × 10^{-9} m^2 s^{-1}) (Colsenet et al., 2005). In the present study, D_{app} follows the sequence D > B > 24 > 34 > 29, ranging from 0.58 (gel D) to 0.44 (gel 29) for Δ = 7.5 ms (Fig. 8). Colsenet et al. (2005) found a D_{app} value of approximately 0.54 for a solution with a whey protein concentration of about 36.7 g/100 g of water at 20 °C and Δ = 7.5 ms (Colsenet et al., 2005). Bouchoux et al. (2012) observed a D_{app} value of around 0.55 for dispersions of casein micelles comprised of native phosphocaseinate and sodium caseinate at a concentration of approximately 225 g/L, using Δ = 7.5 ms at 25 °C (Bouchoux et al., 2012).

D_{app} correlates negatively with dry matter content, as illustrated in Fig. 8, for Δ = 7.5 ms. This result further confirms the obstruction effect of proteins. Despite the slightly higher dry matter content of gel 34 compared to gel 29, the D_{app} value for gel 34 is shorter than for gel 29. This is likely to be caused by the presence of lipids in gel 34, which can impact both dry matter content and the arrangement of the gel structure, as discussed with reference to relaxation times. Fig. 8 shows that gel 29 has the highest dry matter content and the most compact network, resulting in the lowest D_{app} value, consistent with the relaxation measurements. Similar findings have been reported for Cheddar and Mozzarella cheeses, where higher dry matter content was associated with a more tortuous structure and increased restriction of water diffusion (Vogt et al., 2015).

Self-diffusion behavior differs for gels 29, 24, B, and D according to diffusion time (Δ), as illustrated in Fig. 9. This dependence of self-diffusion on Δ is commonly reported in the literature for porous rock and dense colloidal suspensions, indicating that the reservoir is not infinite reflecting a physical barrier effect that impedes the diffusive movements of molecules. The dependence of self-diffusion on Δ can therefore provide information on the average size of the internal spaces in which the liquid molecules are present, as long as Δ is greater than the average molecule-to-barrier distance (Stejskal and Tanner, 1965; Woessner, 1963).

In gel systems 24, 29, B, and D, the dependence of self-diffusion on Δ suggests that the movement of water molecules is limited to a distance ranging from 5 to 35 μm. It indicates a reduction in water diffusion levels within the gels, possibly caused by the movement of molecules between compartments or by molecules encountering barriers that affect their motion. Similar decreases in the water diffusion coefficient with increasing diffusion time have been reported for cheddar and mozzarella cheeses, where the tortuosity of the porous matrix has been proposed as an explanation for this phenomenon (Vogt et al., 2015). However, other studies of casein dispersion and acid gel samples have reported self-diffusion to be independent of the diffusion time (Bouchoux et al., 2012; Colsenet et al., 2005; Mariette et al., 2002).

Interestingly, the self-diffusion coefficient of water in gel 34 appears unaffected by the Δ increments, as shown in Fig. 9. This finding suggests that the structure of gel 34 is less tortuous than those of the other acid gels, with a network that is poorly crosslinked, allowing most of the water molecules in gel 34 to diffuse freely throughout the gel structure without being confined or hindered by barriers or compartments. The

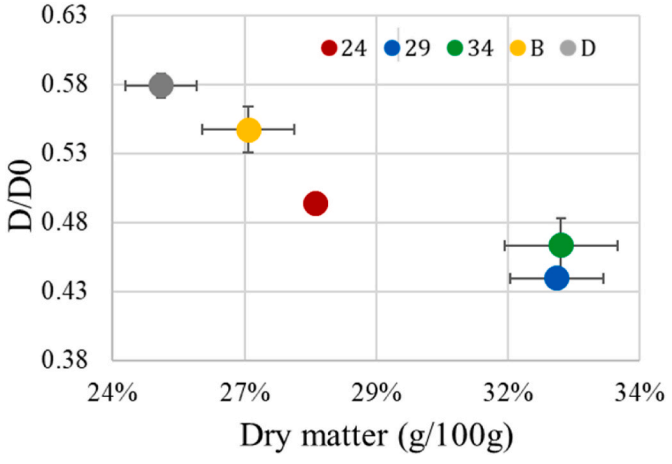

Fig. 8. D/D_0 relative to dry matter content for gels 24, 29,34, B, and D where Δ = 7.5 ms.

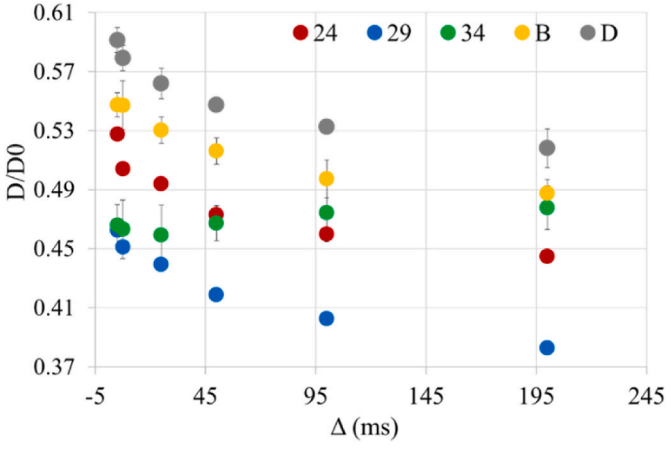

Fig. 9. D/D_0 in relation to different Δ values in gels 24, 29, 34, B, and D centrifuged for 30 min.

literature reports that the interaction between fat globules and the protein matrix is determined by the nature of the surface components of the globules. Where native fat globule membranes fail to interact with casein particles, this serves as a 'structure breaker' (Métais et al., 2006). The opposite occurred in gel 34, where the membrane was formed mainly of casein. This allows us to assume that the fat-protein network interactions were strong, making it harder for casein clusters to shrink and explaining the absence of a restriction effect in gel 34. The opposite was observed by Vogt et al. (2015), who reported that lipid globules influenced the tortuosity of the cheese structure, leading to restricted water movement through the cheese's pores and reducing water diffusion (Vogt et al., 2015).

Comparison of gels D and B in Figs. 8 and 9, clearly shows that gel D has a less compact structure. This is indicated by its higher D_{app} value and slightly lower dry matter content compared to gel B. Consequently is possible to infer that the microparticulated denatured whey proteins, present only in gel D, contributed to a more open protein structure. This conclusion is in line with the relaxation measurements.

4. Conclusions

The MRI approach developed in this paper provides a spatio-temporal account of water content in gels during different draining processes. It also enables quantification of drained serum content for the duration of the experiment. Of particular note is this study's pioneering application of a dedicated amagnetic device designed to monitor the real-time draining processes of acid gels, enabling the assessment of their kinetic evolution.

The analysis of MRI images revealed that gel 34 had the slowest draining kinetics, the highest water content, and a less compact structure at the end of filtration draining (longest T_2). At the other end of the scale, gel 24 displayed the fastest draining rate, similar to gel 29, while gel 29 had the lowest water content and the most compact network (shortest T_2). T_2 values and TD-NMR self-diffusion measurements supported these findings. Gel 34's network was characterized by the presence of melted lipids, impacting its water-holding capacity by hindering casein cluster shrinkage. These correlations with the milk fat content would require further experiments in a future study with more formulations involving different fat content levels to explain the draining phenomenon. Conversely, the organization of gel 29 was more compact, which was attributed to milder thermal treatment and the use of microparticulated denatured whey proteins in its formulation.

Serum draining was slightly faster in gel D than gel B, although the MRI results suggested that the water content of both filtered B and D gels was generally similar at the end of the draining filtration experiment. More comprehensive structural insights were provided by TD-NMR measurements. These revealed that drained gel D (by filtration or centrifugation) had a higher water content and lower dry matter content than drained gel B, suggesting that the structure of gel D was slightly less densely packed. These findings were confirmed by the self-diffusion measurements carried out on samples centrifuged for 30 min and suggest a significant role for the addition of 12.5% microparticulated denatured whey proteins to gel D as a substitute for the casein fraction.

To expand on the interpretation of the T_2 and water content MRI maps, it would be useful to increase certain parameters, such as the number of echoes and recycle delays. For this, bi-exponential fitting data processing would be an appropriate choice and would yield more detailed information on the water distribution in gels. There is a trade-off to be made between the optimization of MRI parameters and the length of experimental time required to monitor the full duration of draining. In the present work, we took the decision to shorten the duration of each experimental run so that more detailed information could be captured on the initial stages of the draining process.

CRediT authorship contribution statement

Tatiana Monaretto: Formal analysis, Investigation, Methodology, Project administration, Writing – original draft. **Stéphane Quellec:** Investigation, Methodology, Software. **Mireille Cambert:** Methodology. **Romain Richoux:** Methodology. **Janushan Christy:** Formal analysis, Software, Visualization. **Patrice Gaborit:** Funding acquisition, Methodology, Project administration, Resources. **Marie-Helene Famelart:** Conceptualization, Methodology, Writing – review & editing. **Corinne Rondeau-Mouro:** Conceptualization, Funding acquisition, Methodology, Project administration, Resources, Supervision, Writing – original draft, Writing – review & editing.

Declaration of competing interest

The authors declare that they have no known competing financial interests or personal relationships that could have appeared to influence the work reported in this paper.

Data availability

The authors do not have permission to share data.

Acknowledgements

This project was coordinated by Actalia (https://www.actalia.eu/) in collaboration with the STLO unit (INRAE) and was funded by the CNIEL (Centre National Interprofessionnel de l'Economie Laitière, grant SCEC6450). The NMR and MRI analyses were carried out using the PRISM NMR facilities (Rennes, France).

Appendix A. Supplementary data

Supplementary data to this article can be found online at https://doi.org/10.1016/j.jfoodeng.2024.112088.

References

Akaike, H., 1998. Information theory and an extension of the maximum likelihood principle. In: Parzen, E., Tanabe, K., Kitagawa, G. (Eds.), Selected Papers of Hirotugu Akaike. Springer New York, New York, NY, pp. 199–213.

Anedda, R., Melis, R., Curti, E., 2021. Quality control in fiore sardo PDO cheese: detection of heat treatment application and production chain by MRI relaxometry and image analysis. Dairy 2 (2), 270–287. https://doi.org/10.3390/dairy2020023.

Bouchoux, A., Schorr, D., Daffé, A., Cambert, M., Gésan-Guiziou, G., Mariette, F., 2012. Molecular mobility in dense protein systems: an investigation through 1H NMR relaxometry and diffusometry. J. Phys. Chem. B 116 (38), 11744–11753. https://doi.org/10.1021/jp306078k.

Callaghan, P.T., Jolley, K.W., Humphrey, R.S., 1983. Diffusion of fat and water in cheese as studied by pulsed field gradient nuclear magnetic resonance. J. Colloid Interface Sci. 93 (2), 521–529. https://doi.org/10.1016/0021-9797(83)90436-8.

Chaland, B., Mariette, F., Marchal, P., De Certaines, J., 2000. 1H nuclear magnetic resonance relaxometric characterization of fat and water states in soft and hard cheese. J. Dairy Res. 67 (4), 609–618. https://doi.org/10.1017/s0022029900004398.

Chen, Y., MacNaughtan, W., Jones, P., Yang, Q., Foster, T., 2020. The state of water and fat during the maturation of Cheddar cheese. Food Chem. 303, 125390 https://doi.org/10.1016/j.foodchem.2019.125390.

Colsenet, R., Mariette, F., Cambert, M., 2005. NMR relaxation and water self-diffusion studies in whey protein solutions and gels. J. Agric. Food Chem. 53 (17), 6784–6790. https://doi.org/10.1021/jf050162k.

Daviau, C., Pierre, A., Famelart, M.-H., Goudédranche, H., Jacob, D., Garnier, M., Maubois, J.-L., 2000. Characterisation of whey drainage kinetics during soft cheese manufacture in relation with the physicochemical and technological factors, pH at renneting, casein concentration and ionic strength of milk. Lait 80 (4), 417–432. https://doi.org/10.1051/lait:2000135.

Gianferri, R., D'Aiuto, V., Curini, R., Delfini, M., Brosio, E., 2007. Proton NMR transverse relaxation measurements to study water dynamic states and age-related changes in Mozzarella di Bufala Campana cheese. Food Chem. 105 (2), 720–726. https://doi.org/10.1016/j.foodchem.2007.01.005.

Hansen, C.L., Rinnan, A., Engelsen, S.B., Janhøj, T., Micklander, E., Andersen, U., van den Berg, F., 2010. Effect of gel firmness at cutting time, pH, and temperature on rennet coagulation and syneresis: an in situ 1H NMR relaxation study. J. Agric. Food Chem. 58 (1), 513–519. https://doi.org/10.1021/jf902264y.

Hills, B.P., Takacs, S.F., Belton, P.S., 1990. A new interpretation of proton NMR relaxation time measurements of water in food. Food Chem. 37 (2), 95–111. https://doi.org/10.1016/0308-8146(90)90084-H.

Hinrichs, R., Götz, J., Noll, M., Wolfschoon, A., Eibel, H., Weisser, H., 2004. Characterisation of the water-holding capacity of fresh cheese samples by means of low resolution nuclear magnetic resonance. Food Res. Int. 37 (7), 667–676. https://doi.org/10.1016/j.foodres.2004.02.005.

Kuo, M.I., Anderson, M.E., Gunasekaran, S., 2003. Determining effects of freezing on pasta filata and non-pasta filata mozzarella cheeses by nuclear magnetic resonance imaging. J. Dairy Sci. 86 (8), 2525–2536. https://doi.org/10.3168/jds.S0022-0302(03)73847-8.

Le Dean, A., Mariette, F., Marin, M., 2004. 1H nuclear magnetic resonance relaxometry study of water state in milk protein mixtures. J. Agric. Food Chem. 52 (17), 5449–5455. https://doi.org/10.1021/jf030777m.

Lucey, J.A., 2002. Formation and physical properties of milk protein gels. J. Dairy Sci. 85, 281–294. https://doi.org/10.3168/jds.s0022-0302(02)74078-2.

Lucey, J.A., 2017. Formation, structural properties, and rheology of acid-coagulated milk gels. In: McSweeney, P.L.H., Fox, P.F., Cotter, P.D., Everett, D.W. (Eds.), Cheese, vol. 85. Academic Press, pp. 179–197.

Lucey, J.A., Singh, H., 1997. Formation and physical properties of acid milk gels: a review. Food Res. Int. 30 (7), 529–542. https://doi.org/10.1016/S0963-9969(98)00015-5.

Mariette, F., 2004. Relaxation RMN et IRM : un couplage indispensable pour l'étude des produits alimentaires. Compt. Rendus Chem. 7 (3), 221–232. https://doi.org/10.1016/j.crci.2003.11.004.

Mariette, F., 2006a. NMR imaging of dairy products. In: Webb, G.A. (Ed.), Modern Magnetic Resonance. Springer Netherlands, Dordrecht, pp. 1801–1806.

Mariette, F., 2006b. NMR relaxation of dairy products. In: Webb, G.A. (Ed.), Modern Magnetic Resonance. Springer Netherlands, Dordrecht, pp. 1697–1701.

Mariette, F., 2017. NMR relaxometry and imaging of dairy products. In: Webb, G.A. (Ed.), Modern Magnetic Resonance. Springer International Publishing, Cham, pp. 1–23.

Mariette, F., Cambert, M., Franconi, F., Marchal, P., 1999. Les produits alimentaires et l'eau. Nantes, France. Paper presented at the Agoral 99.

Mariette, F., Guillement, J.P., Tellier, C., Marchal, P., 1996. Continuous relaxation time distribution decomposition by mem. In: R, D.N. (Ed.), Data Handling in Science and Technology, vol. 18. Elsevier, Amsterdam, NLD, pp. 218–234.

Mariette, F., Tellier, C., Brule, G., Marchal, P., 1993. Multinuclear NMR study of the pH dependent water state in skim milk and caseinate solutions. J. Dairy Res. 60 (2), 175–188. https://doi.org/10.1017/S0022029900027497.

Mariette, F., Topgaard, D., Jönsson, B., Soderman, O., 2002. 1H NMR diffusometry study of water in casein dispersions and gels. J. Agric. Food Chem. 50 (15), 4295–4302. https://doi.org/10.1021/jf0115948.

Métais, A., Cambert, M., Riaublanc, A., Mariette, F., 2006. Influence of fat globule membrane composition on water holding capacity and water mobility in casein rennet gel: a nuclear magnetic resonance self-diffusion and relaxation study. Int. Dairy J. 16 (4), 344–353. https://doi.org/10.1016/j.idairyj.2005.03.011.

Mulas, G., Anedda, R., Longo, D.L., Roggio, T., Uzzau, S., 2016. An MRI method for monitoring the ripening of Grana Padano cheese. Int. Dairy J. 52, 19–25. https://doi.org/10.1016/j.idairyj.2015.08.011.

Pocan, P., Oztop, M.H., 2022. Chapter 10 - low-field time-domain nuclear magnetic resonance applied to dairy foods. In: Cruz, A.G.d., Ranadheera, C.S., Nazzaro, F., Mortazavian, A.M. (Eds.), Dairy Foods. Woodhead Publishing, pp. 215–232.

Salami, S., Rondeau-Mouro, C., van Duynhoven, J., Mariette, F., 2013. PFG-NMR self-diffusion in casein dispersions: effects of probe size and protein aggregate size. Food Hydrocolloids 31 (2), 248–255. https://doi.org/10.1016/j.foodhyd.2012.10.020.

SAS Institute Inc, 2015. User's Guide (Version SAS/STAT® 14.1). SAS Institute Inc.

Smith, J.R., Vogt, S.J., Seymour, J.D., Carr, A.J., Codd, S.L., 2017. Probing water migration in Mozzarella cheese during maturation and heating utilizing magnetic resonance techniques. J. Food Eng. 198, 1–6. https://doi.org/10.1016/j.jfoodeng.2016.11.010.

Stejskal, E.O., Tanner, J.E., 1965. Spin diffusion measurements: spin echoes in the presence of a time-dependent field gradient. J. Chem. Phys. 42 (1), 288–292. https://doi.org/10.1063/1.1695690.

Tanner, J.E., 1970. Use of the stimulated echo in NMR diffusion studies. J. Chem. Phys. 52 (5), 2523–2526. https://doi.org/10.1063/1.1673336.

Tellier, C., Mariette, F., Guillement, J.P., Marchal, P., 1993. Evolution of water proton nuclear magnetic relaxation during milk coagulation and syneresis: structural implications. J. Agric. Food Chem. 41 (12), 2259–2266. https://doi.org/10.1021/jf00036a007.

Vasbinder, A.J., Alting, A.C., de Kruif, K.G., 2003. Quantification of heat-induced casein–whey protein interactions in milk and its relation to gelation kinetics. Colloids Surf. B Biointerfaces 31 (1), 115–123. https://doi.org/10.1016/S0927-7765(03)00048-1.

Vogt, S.J., Smith, J.R., Seymour, J.D., Carr, A.J., Golding, M.D., Codd, S.L., 2015. Assessment of the changes in the structure and component mobility of Mozzarella and Cheddar cheese during heating. J. Food Eng. 150, 35–43. https://doi.org/10.1016/j.jfoodeng.2014.10.026.

Wang, X., Zhao, Z., 2022. Acid-induced gelation of milk : formation mechanism, gel characterization, and influence of different techniques. In: Ibrahim, S.A. (Ed.), Dairy Processing - from Basics to Advances. IntechOpen, Rijeka.

Woessner, D.E., 1963. NMR spin-echo self-diffusion measurements on fluids undergoing restricted diffusion. J. Phys. Chem. 67 (6), 1365–1367. https://doi.org/10.1021/j100800a509.